Automatic diagnosis of COVID-19 and pneumonia using FBD method

Pradeep Kumar Chaudhary and Ram Bilas Pachori
Discipline of Electrical Engineering
Indian Institute of Technology Indore
Indore - 453552, India
Email: phd1801202005, pachori@iiti.ac.in

2020 IEEE International Conference on Bioinformatics and Biomedicine (BIBM) 978-1-7281-6215-7/20/$31.00 ©2020 IEEE DOI: 10.1109/BIBM49941.2020.9313252

***Abstract*—Novel coronavirus (COVID-19) is spreading rapidly and has taken millions of lives worldwide. A medical study has shown that COVID-19 affects the lungs of patients and shows the symptoms of pneumonia. X-ray images with artificial intelligence (AI) can be useful for a fast and accurate diagnosis of COVID-19. It can also solve the problem of less testing kits and fewer doctors. In this paper, we have introduced the Fourier-Bessel series expansion-based dyadic decomposition (FBD) method for image decomposition. This FBD is used to decompose an X-ray image into subband images. Obtained subband images are then fed to ResNet50 pre-trained convolution neural network (CNN) individually. Deep features from each CNN are ensembled using operations, namely; maxima (max), minima (min), average (avg), and fusion (fus). Ensemble CNN features are then fed to the softmax classifier. In the study, a total of 750 X-ray images are collected. Out of 750 X-ray images, 250 images are of pneumonia patients, 250 of COVID-19 patients, and 250 healthy subjects. The proposed model has provided an overall accuracy of 98.6% using fus ensemble ResNet-50 CNN model.**

Keywords*— *Fourier-Bessel series expansion (FBSE), Image decomposition, Corona virus, Pneumonia, X-ray image.

I. Introduction

Novel coronavirus (COVID-19) is the result of severe acute respiratory syndrome coronavirus 2 (SARS-COV-2). The symptoms of COVID-19 ranges from dry cough, sore throat, loss of taste, and fever to organ failure, pneumonia, and acute respiratory distress syndrome [1], [2]. Another challenge countries are facing along with COVID-19 is the lack of the testing kits. So there is a requirement of finding new ways by which the diagnosis of COVID-19 becomes fast and accurate. The studies found that X-ray and computer tomography (CT) scan images can be tools that can diagnose pneumonia caused by COVID-19 [3]. The idea is to use image processing techniques and artificial intelligence (AI) to get contact-less testing.

Some research works have been done for diagnosing COVID-19 with X-ray and CT images using AI [4], [5], [6]. Xu et al. [7] extracted infected region from CT scan image using a pre-trained 3D-convolution neural network (CNN). These regions are fed to CNN for three classes (COVID-19, Influenza-A-viral-pneumonia, and healthy) classification. The CT scans have been utilized in [8] to detect COVID-19 cases, where all slices of CT scans are fed to the CNN model separately. The output from each model is aggregated by applying a max-pooling process. Wang and Wong [9], use a pre-train CNN model which was first trained with ImageNet dataset [10], which are then fine-tuned with X-ray images to classify subjects as COVID-19, normal, bacterial infection, and none-COVID-19 viral. Similar work was done by Sethy and Behera [11], where several CNN models are trained on X-ray images, and a support vector machine (SVM) classifier used to detect COVID-19. Research has found that a CT scan can be the better tool for COVID-19 diagnosis compared to X-ray images [3]. But the drawback of using a CT scan is that it takes more time than X-ray imaging. High-quality CT scanners are usually not available in rural or underdeveloped regions, making this time-consuming process [12].

This paper uses a new multi-resolution analysis technique for image decomposition, called Fourier-Bessel series expansion (FBSE) based dyadic decomposition (FBD). The method is inspired by multi-frequency scale 2D-FBSE-empirical wavelet transform (EWT) (2D-FBSE-EWT) [13], where multi-frequency scale (dyadic frequency scale) FBSE spectrum is used for boundaries detection in EWT method. FBD is used to decompose X-ray images to get subband images. Each subband is fed to the ResNet-50 CNN individually. Deep features are then extracted from the last fully connected layer of each ResNet-50 CNN. These features are then ensembled using the operations, namely maximum (max), minimum (min), average (avg), and fusion (fus) [14]. Ensemble features are then fed to a softmax classifier to classify pneumonia caused by COVID-19 and other pneumonia.

The rest of the paper is organized as follows: Section 2 presents the paper's database and briefly introduces the FBD. The method proposed for the automated diagnosis of COVID-19 and pneumonia is explained briefly in Section 3. Section 4 provides experimental results and discussion. Conclusion has been provided in Section 5.

II. Database and proposed FBD

A. Database

In this paper, 750 images are collected from two databases. 250 X-ray images are downloaded from URL: https://github.com/ieee8023/covid-chestxray-dataset. Images are of pneumonia caused by COVID-19 [15]. For 250 healthy and 250 viral pneumonia X-ray images, the kaggle repository database called "Chest X-Ray Images" [16] is used.

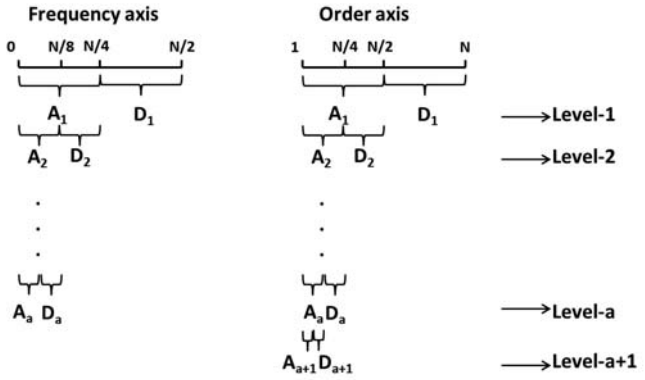

Fig. 1: Dyadic decomposition in frequency and order axis.

B. FBD method

FBD is a dyadic decomposition method motivated by the discrete wavelet transform (DWT) [17], [18] and multi-frequency scale 2D-FBSE-EWT method. FBD uses the FBSE spectrum instead of the discrete Fourier transform (DFT) spectrum, so it provides plus one level of decomposition compared to DWT. FBSE provides N (length of signal) different FBSE coefficients, whereas DFT provides only $N/2$ different coefficients. So if DWT can provide maximum level-a (Where 'a' represent maximum level of decomposition by DWT) decomposition, then FBD can provide a maximum level-a+1 number of decomposition. So it implies that FBD can provide better multi-resolution analysis compared to DWT. Fig.1 shows the dyadic operation of DWT (frequency axis) and FBD (order axis). A_i and D_i represent level-i approximate and detailed components of the transforms.

In [19], authors have shown how by filtering operation, the amplitude and frequency functions of the signal are changed and also propose FBSE based grouping process to resolve it. So in FBD, instead of using filters, i.e., low pass filter (LPF) and high pass filter (HPF) as done in DWT, FBSE based grouping operation is used. Another advantage of using FBSE is that FBSE uses Bessel functions as a basis for signal representation, which are non-stationary. So FBSE can do better analysis of non-stationary signals as compared to the transform uses stationary basis function [20], [21]. Due to these reasons FBSE has been used in many areas [22], [23], [24].

In this work, both order zero [25], [26] and order one FBSE [24] are used for analysis based on FBD method. The mathematical expressions corresponding to order zero FBSE and order one FBSE of signal $x(l)$ of length L are shown in equations (1) and (2) respectively [13].

$$x(l) = \sum_{m=1}^{L} a_m J_0\left(\frac{\xi_m l}{L}\right), \qquad l = 0, 1, ..., L-1 \quad (1)$$

$$x(l) = \sum_{m=1}^{L} b_m J_1\left(\frac{\zeta_m l}{L}\right), \qquad l = 0, 1, ..., L-1 \quad (2)$$

Where a_m and b_m are order zero and order one FBSE coefficients respectively, which are mathematically expressed as [26], [24],

$$a_m = \frac{2}{L^2(J_1(\xi_m))^2} \sum_{l=0}^{L-1} lx(l) J_0\left(\frac{\xi_m l}{L}\right) \quad (3)$$

$$b_m = \frac{2}{L^2(J_0(\zeta_m))^2} \sum_{l=0}^{L-1} lx(l) J_1\left(\frac{\zeta_m l}{L}\right) \quad (4)$$

$J_0(.)$ and $J_1(.)$ are order zero and order one Bessel functions. ξ_m denotes the m^{th} positive root of equation $J_0(.) = 0$. Similarly ζ_m denotes the m^{th} positive root of equation $J_1(.) = 0$ [26]. By FBSE, signal is transformed from l (spatial or time) domain to m (order) domain. Another advantage of using FBD is that any level of decomposition can be obtained in a single step. For example, the level-3 approximation signal can be obtained by grouping the FBSE coefficients from range m (order)=1 to m=$N/8$. On the other hand, DWT requires three down-sampling and three filtering operations at the decomposition stage and three up-sampling and three filtering operations at the reconstruction stage.

III. Proposed methodology for COVID-19 and pneumonia diagnosis

The block diagram of the proposed methodology is shown in Fig. 2. In the pre-processing stage, the X-ray image is first resized to 512×512 and then contrast limited adaptive histogram equalization (CLAHE) [27] applied for contrast enhancement, followed by image negative. Image negative of X-ray image provides a better representation of lesion [28]. Fig. 3 (a) shows the raw X-ray image, Fig. 3 (b) shows the CLAHE image, and Fig. 3 (c) shows the image negative. Then FBD is used to decompose pre-processed images into subband images. Instead of extracting features arbitrarily from the subband image, each decomposed subband image is fed to ResNet-50 CNN to extract deep features. Deep features from each CNN are ensembled and fed to a softmax classifier to classify pneumonia due to COVID-19 and other pneumonia.

A. 2D-FBD method

The block diagram of FBD for level-1 image decomposition is shown in Fig. 4. LPG represents the low pass grouping of the first $N/2$ 2D-FBSE coefficients, HPG represents the high pass grouping of the last $N/2$ 2D-FBSE coefficients. 2D-FBSE coefficients can be obtained by applying FBSE row-wise, followed by FBSE column-wise [29]. LPG row and HPG row represent LPG and HPG row-wise. Similarly, the LPG column and HPG column represent LPG and HPG column-wise, respectively. LL, LH, HL, and HH subbands images can be obtained by applying 2D- inverse Fourier-Bessel series expansion (2D-IFBSE) to the four grouped 2D-FBSE coefficients (at each decomposition level). Eqs. (1) and (2) are the expressions of order zero and order one 1D-IFBSE. 2D-IFBSE can be obtained by applying 1D-FBSE column wise, followed by 1D-FBSE row wise.

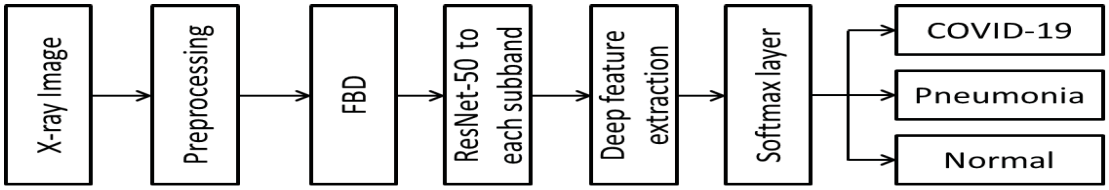

Fig. 2: Proposed framework for automated diagnosis of COVID-19 and pneumonia.

Fig. 3: Preprocessing of X-ray images, where (i) Raw X-ray image, (ii) CLAHE image, and (iii) Image negative.

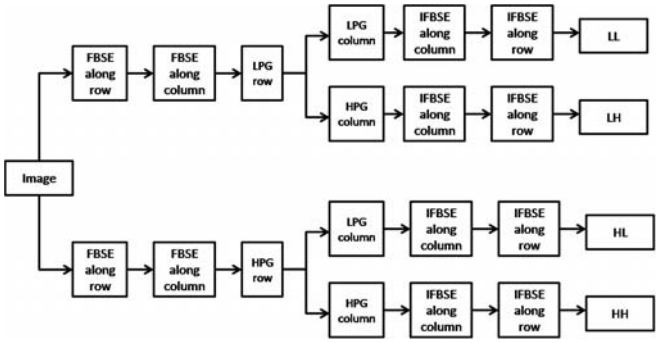

Fig. 4: Block diagram of level-1 image decomposition using FBD.

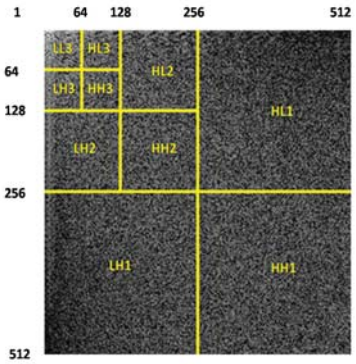

Fig. 5: Order-space plot of X-ray image which is shown in Fig. 3 (iii).

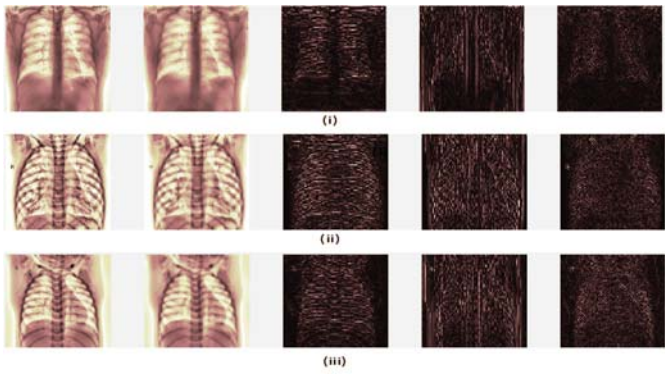

Fig. 6: X-ray image (pseudo colour image) and its decomposed components: LL3, HL3, LH3, and HH3 of (i) COVID-19, (ii) Pneumonia, and (iii) Normal subject obtained using FBD.

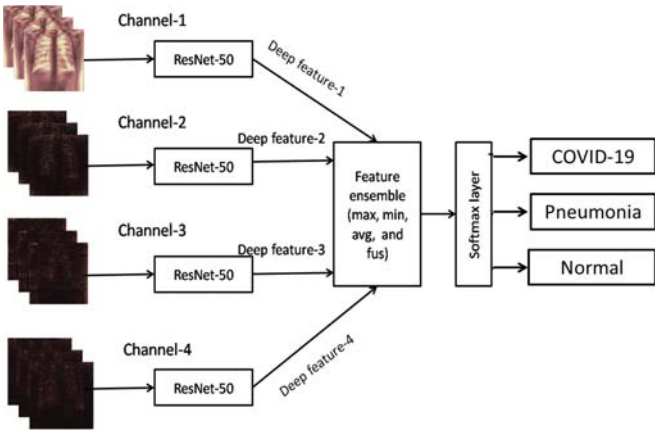

Fig. 7: Block diagram of ensemble ResNet-50 CNN model for level-1 decomposed subband images.

Fig. 5 is a order zero 2D-FBSE order-space plane (log of 2D-FBSE coefficients) of preprocessed image. Blocks in the order-space plane represent a group of coefficients to get a different level of decomposition. Number with LL, LH, HL, and HH represents the level of decomposition. In Fig. 6, the first row shows an X-ray image of the COVID-19 subject, followed with its four (LL3, LH3, HL3, and HH3) decomposed images, similarly second and third rows are of pneumonia and normal subjects respectively, followed by their four decomposed components.

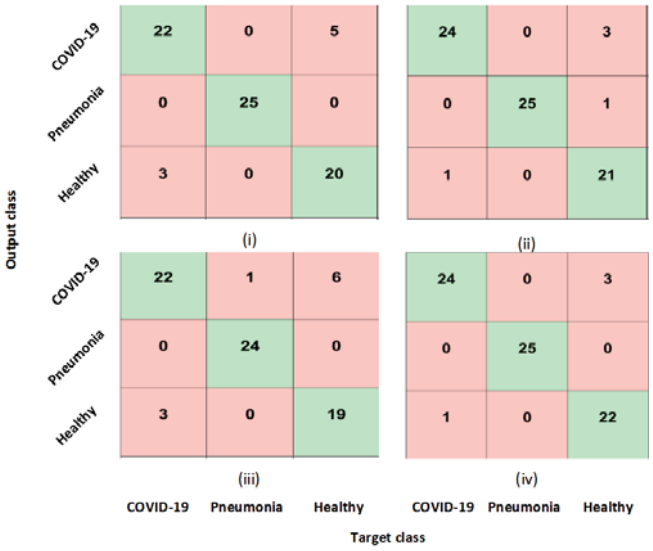

Fig. 8: Confusion matrix of (i) Max, (ii) Min, (iii) Avg, and (iv) Fus ensemble Resnet-50 CNN model for FBD level-1 decomposed images.

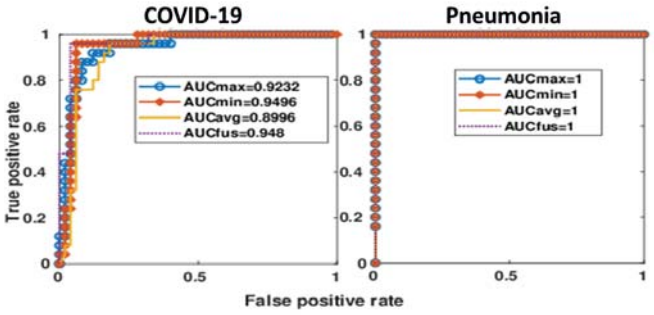

Fig. 9: ROC plot of max, min, avg and fus ensemble ResNet-50 CNN model for (i) COVID-19 and (ii) Pneumonia class of FBD level-1 decomposed images.

B. Ensemble ResNet-50 CNN model

The ResNet-50 is a CNN which is 50 layers deep [30]. This network is trained on ImageNet [10] database, having millions of images and 1000 object categories. The advantage of using a pre-train network is that it is trained with a massive database, so the deep features will be of higher quality. Based on the transfer learning approach, one can transfer this knowledge of pre-train networks to perform other tasks. Using the transfer learning technique, the initial 49 layers of ResNet-50 are frozen, and the softmax layer of 1000 nodes is replaced by a softmax layer of 3 nodes (since we are using three-class). Now this network is trained with our database.

From a trained network, deep features are extracted from the last fully connected layer of ResNet-50. Deep features from each channel is ensembled using maxima (max), minima (min), average (avg), and fusion (fus) operations. This ensemble feature is then used to train the three node softmax layer. Fig. 7 shows the block diagram of the ensemble ResNet-50 CNN model for level-1 decomposition.

IV. Results and Discussions

In this paper, order zero and order one FBD are used for the diagnosis of pneumonia due to COVID-19 and pneumonia. For this total of 750 X-ray images are used, with 250 images of each class (COVID-19, pneumonia, and healthy). Input images are pre-processed and then decomposed using the FBD method. The obtained subbands are then fed to pre-trained ResNet-50 CNN individually. For training CNN, stochastic gradient descent with momentum algorithm is used. The initial learning rate and the number of epochs are fixed to 3×10^{-4} and 6 respectively. 85% of data is used for training, 5% data for validation, and 10% of data is used for testing purposes. Deep features are then extracted from the last fully connected layer of each ResNet-50. These deep features are then ensembled using max, min, avg, and fus operations and finally fed to the softmax classifier for classification. This process is performed with order zero FBD, order one FBD, and 2D-DWT subband images, and the results of all the methods are then compared. For the 2D-DWT method, one issue is selecting the best mother wavelet for a particular application. So, for 2D-DWT decomposition, we have arbitrarily considered three different mother wavelets: Haar, Symlets 4 (sym), and Daubechies 4 (db) wavelets. Then an analysis of all the decomposition methods is done for level-1, level-2, and level-3.

Parameters used for checking the classifier performance is accuracy, sensitivity, and specificity, and area under the curve (AUC) of receiver operating characteristic (ROC) curve [33]. Mathematical expressions of accuracy, sensitivity, and specificity are shown below [34].

$$\text{Accuracy} = \frac{\text{TP+TN}}{\text{TP+TN+FP+FN}} \ \% \tag{5}$$

$$\text{Sensitivity} = \frac{\text{TP}}{\text{TP+FN}} \ \% \tag{6}$$

$$\text{Specificity} = \frac{\text{TN}}{\text{TN+FP}} \ \% \tag{7}$$

True positive, true negative, false positive, and false negative have been denoted by TP, TN, FP, and FN respectively. ROC is a curve ploted between the TP rate and the FP rate. AUC of ROC tells how much model is capable of distinguishing between classes. Sensitivity, specificity, and AUC of ROC obtained by our method for each ensemble classifier model are shown in Table I. Table I represents the performance comparison of 2D-DWT (Haar, db, and sym), order zero FBD, and order one FBD for level-1, level-2, and level-3 decompositions. Term Specov, Sencov, and AUCcov are sensitivity, specificity, and ROC AUC of COVID-19. Similarly, Spepne, Senpne, and AUCpne are sensitivity, specificity, and ROC AUC of pneumonia. By comparing the table, it can be seen that level-1 decomposition has provided better performance as compared to level-2 and level-3 decompositions. Along with that, on the

TABLE I: Performance of all models for level-1, level-2, and level-3 decompositions.

Classifier model	Sencov19 (%)	Senpne (%)	Specov (%)	Spepne (%)	Accuracy (%)	AUCcov	AUCpne
				level-1			
For DWT (Haar)							
Max	96	96	94	100	93	0.97	0.99
Min	84	96	94	100	89.33	0.96	1
Avg	76	96	94	100	86.66	0.93	0.96
Fus	92	100	94	100	93.33	0.96	1
For DWT (db)							
Max	88	96	92	100	89.33	0.93	0.99
Min	80	96	92	100	88	0.93	1
Avg	84	92	90	100	86.6	0.92	0.95
Fus	92	100	92	100	92	0.94	1
For DWT (sym)							
Max	84	100	90	100	88	0.91	1
Min	76	96	92	100	85.33	0.90	0.99
Avg	84	92	88	96	82.66	0.94	0.98
Fus	88	100	90	100	89.33	0.94	1
For order zero FBD							
Max	88	100	90	100	89.33	0.92	1
Min	96	100	94	98	93.33	0.94	1
Avg	88	96	86	100	86.66	0.89	1
Fus	96	100	94	100	98.61	0.94	1
For order one FBD							
Max	88	96	98	98	93.3	0.91	0.99
Min	80	100	98	94	92	0.90	0.99
Avg	72	92	94	94	85	0.92	0.93
Fus	88	100	98	98	94	0.93	0.99
				level-2			
For DWT (Haar)							
Max	88	96	92	98	89.33	0.93	0.99
Min	92	92	92	98	89.33	0.94	0.99
Avg	72	56	72	90	62.66	0.75	0.71
Fus	84	96	90	98	86.66	0.93	0.99
For DWT (db)							
Max	84	100	94	98	90.66	0.92	1
Min	92	100	92	98	90.66	0.94	1
Avg	76	88	86	98	82.6	0.77	0.91
Fus	84	100	92	98	89.33	0.91	1
For DWT (sym)							
Max	80	92	86	100	81.33	0.90	1
Min	84	88	86	100	81.33	0.88	0.95
Avg	84	76	82	96	78.66	0.82	0.88
Fus	84	96	84	100	84	0.87	0.99
For order zero FBD							
Max	96	100	94	100	94	0.96	1
Min	96	96	88	100	89.33	0.93	0.99
Avg	80	84	82	98	78.66	0.80	0.88
Fus	92	96	88	100	89.33	0.95	1
For order one FBD							
Max	84	92	94	98	90.7	0.96	0.99
Min	92	84	88	100	89.33	0.95	0.98
Avg	76	88	86	98	82.66	0.63	0.68
Fus	92	92	94	100	93.33	0.96	0.99
				level-3			
For DWT (Haar)							
Max	88	100	90	96	89.33	0.91	1
Min	92	100	90	100	90.66	0.94	1
Avg	60	92	90	76	74.66	0.80	0.86
Fus	92	96	90	98	90.66	0.95	0.99
For DWT (db)							
Max	88	92	86	98	85.33	0.91	0.99
Min	76	88	86	96	78.66	0.88	0.96
Avg	68	76	70	90	66.6	0.7	0.8
Fus	88	92	88	96	84	0.92	0.98
For DWT (sym)							
Max	80	92	86	100	81.33	0.90	1
Min	84	88	86	100	81.33	0.88	0.95
Avg	84	76	82	96	78.66	0.82	0.88
Fus	84	96	84	100	84	0.87	0.99
For order zero FBD							
Max	84	100	90	100	88	0.93	1
Min	88	100	92	100	90.66	0.94	1
Avg	72	76	76	96	70.66	0.73	0.86
Fus	88	100	90	100	89.33	0.91	1
For order one FBD							
Max	92	92	94	100	92	0.97	0.99
Min	84	92	92	98	89.33	0.98	0.99
Avg	72	76	76	96	70.6	0.51	0.86
Fus	84	96	92	98	89.3	0.97	0.99

TABLE II: Performance comparison of proposed method with different works which are used for identification of COVID-19.

Reference	Images	Number of classes	Sensitivity (%)	Specificity (%)	Accuracy (%)	AUC
[31]	1531	2	90	87	96	0.95
[4]	100	2	100	100	98	-
[32]	50	2	-	-	90	-
[5]	1427	3	98.66	96.46	96.78	-
[11]	50	2	97	93	95.38	-
Proposed method	**750**	**3**	**96**	**94**	**98.66**	**0.94**

basis of overall accuracy, order zero FBD has provided better performance, followed by order one FBD, DWT with Haar, DWT with db, and finally, DWT with sym. At level-3 best overall accuracy is 92%, and it is obtained by order one FBD decomposition with max ensemble ResNet-50 CNN model. At level-2 best overall accuracy is 94%, and it is obtained by order zero FBD decomposition with max ensemble ResNet-50 CNN model. At level-1 best overall accuracy is 98.6%, and it is obtained by order zero FBD decomposition with fus ensemble ResNet-50 CNN model. Figs. 8 and 9 show confusion and ROC plot of FBD (level-1) decomposition with max, min, avg, and fus ensemble ResNet-50 CNN model. Sensitivity, specificity, and AUC of ROC of COVID-19 class using the proposed method (level-1 FBD with fus ensemble ResNet-50) is 96%, 94%, and 0.94. Similarly, sensitivity, specificity, and AUC of ROC of pneumonia class is 100% and 100%, and 1 and the overall accuracy of the proposed model is 98.66%. Table II shows the performance comparison of the proposed method with some of the methodologies present in the literature. Our proposed method has provided higher classification accuracy among them.

V. Conclusion

COVID-19 pandemic has shocked the world and still threatening many lives of the people. Due to the leak of testing machines, there is a requirement of new techniques by which COVID-19 diagnosis can become fast and accurate. In this work, we have introduced a new order zero FBD and order one FBD method for image decomposition, which is FBSE based dyadic decomposition (without using a filter). We illustrated how by using the FBSE spectrum, we get one extra level of decomposition compared to the DFT spectrum, i.e., get better multi-resolution representation. We also show how by using FBD, one can get any level of decomposed subband images or signal in a single step.

In this work, order zero and order one 2D-FBD are used to decompose the X-ray image into subband images. Each subband is used to train ResNet-50 CNN individually. Deep features from each CNN are ensembled using max, min, avg, and fus operations and finally fed to a softmax classifier. The same process has also been done with 2D-DWT subband images obtained by using Haar, db, and sym as mother wavelets and results from all the methods are compared. From the comparison, it can be concluded that order zero FBD (level-1) with fus ensemble ResNet-50 CNN model has provided better performance, with overall accuracy equal to 98.66%.

References

[1] T. Mahmud, M. A. Rahman, and S. A. Fattah, "Covxnet: A multi-dilation convolutional neural network for automatic covid-19 and other pneumonia detection from chest X-ray images with transferable multi-receptive feature optimization," *Computers in Biology and Medicine*, vol. 122, p. 103869, 2020.

[2] "Coronavirus," Encyclopædia Britannica, Aug. 2020. [Online]. Available: https://www.britannica.com/science/coronavirus-virus-group

[3] Y. Fang, H. Zhang, J. Xie, M. Lin, L. Ying, P. Pang, and W. Ji, "Sensitivity of chest CT for COVID-19: comparison to RT-PCR," *Radiology*, p. 200432, 2020.

[4] A. Narin, C. Kaya, and Z. Pamuk, "Automatic detection of coronavirus disease (covid-19) using X-ray images and deep convolutional neural networks," *arXiv preprint arXiv:2003.10849*, 2020.

[5] I. D. Apostolopoulos and T. A. Mpesiana, "Covid-19: automatic detection from X-ray images utilizing transfer learning with convolutional neural networks," *Physical and Engineering Sciences in Medicine*, p. 1, 2020.

[6] K. K. Bressem, L. Adams, C. Erxleben, B. Hamm, S. Niehues, and J. Vahldiek, "Comparing different deep learning architectures for classification of chest radiographs," *arXiv preprint arXiv:2002.08991*, 2020.

[7] C. Butt, J. Gill, D. Chun, and B. A. Babu, "Deep learning system to screen coronavirus disease 2019 pneumonia," *Applied Intelligence*, p. 1, 2020.

[8] L. Li, L. Qin, Z. Xu, Y. Yin, X. Wang, B. Kong, J. Bai, Y. Lu, Z. Fang, Q. Song *et al.*, "Artificial intelligence distinguishes covid-19 from community acquired pneumonia on chest CT," *Radiology*, p. 200905, 2020.

[9] L. Wang and A. Wong, "Covid-net: A tailored deep convolutional neural network design for detection of covid-19 cases from chest radiography images," *arXiv preprint arXiv:2003.09871*, 2020.

[10] A. Krizhevsky, I. Sutskever, and G. E. Hinton, "Imagenet classification with deep convolutional neural networks," in *Advances in Neural Information Processing Systems*, 2012, pp. 1097–1105.

[11] P. K. Sethy and S. K. Behera, "Detection of coronavirus disease (covid-19) based on deep features," *Preprints*, vol. 2020030300, p. 2020, 2020.

[12] P. Afshar, S. Heidarian, F. Naderkhani, A. Oikonomou, K. N. Plataniotis, and A. Mohammadi, "Covid-caps: A capsule network-based framework for identification of covid-19 cases from X-ray images," *arXiv preprint arXiv:2004.02696*, 2020.

[13] P. K. Chaudhary and R. B. Pachori, "Automatic diagnosis of glaucoma using two-dimensional fourier-bessel series expansion based empirical wavelet transform," *Biomedical Signal Processing and Control*, vol. 64, p. 102237, 2021. [Online]. Available: http://www.sciencedirect.com/science/article/pii/S1746809420303670

[14] H. Fu, J. Cheng, Y. Xu, C. Zhang, D. W. K. Wong, J. Liu, and X. Cao, "Disc-aware ensemble network for glaucoma screening from fundus image," *IEEE Transactions on Medical Imaging*, vol. 37, no. 11, pp. 2493–2501, 2018.

[15] J. P. Cohen, P. Morrison, and L. Dao, "Covid-19 image data collection," *arXiv preprint arXiv:2003.11597*, 2020.

[16] "Kaggle chest X-ray images (pneumonia) dataset,," 2018. [Online]. Available: https://www.kaggle.com/paultimothymooney/chest-xray-pneumonia

[17] M. J. Shensa, "The discrete wavelet transform: wedding the a trous and mallat algorithms," *IEEE Transactions on Signal Processing*, vol. 40, no. 10, pp. 2464–2482, 1992.

[18] S. Mallat and S. Zhong, "Characterization of signals from multiscale edges," *IEEE Transactions on Pattern Analysis and Machine Intelligence*, vol. 14, no. 7, pp. 710–732, 1992.

[19] R. B. Pachori and P. Sircar, "Analysis of multicomponent AM-FM signals using FB-DESA method," *Digital Signal Processing*, vol. 20, no. 1, pp. 42–62, 2010.

[20] R. B. Pachori and P. Sircar., "Non-stationary signal analysis: Methods based on Fourier-Bessel representation," *LAP LAMBERT Academic Publishing, Germany*, vol. 630, 2010.

[21] A. Bhattacharyya, L. Singh, and R. B. Pachori, "Fourier–Bessel series expansion based empirical wavelet transform for analysis of non-stationary signals," *Digital Signal Processing*, vol. 78, pp. 185–196, 2018.

[22] V. Gupta and R. B. Pachori, "Epileptic seizure identification using entropy of FBSE based EEG rhythms," *Biomedical Signal Processing and Control*, vol. 53, p. 101569, 2019.

[23] R. B. Pachori and P. Sircar, "A new technique to reduce cross terms in the Wigner distribution," *Digital Signal Processing*, vol. 17, no. 2, pp. 466–474, 2007.

[24] K. Gopalan, T. R. Anderson, and E. J. Cupples, "A comparison of speaker identification results using features based on cepstrum and Fourier-Bessel expansion," *IEEE Transactions on Speech and Audio Processing*, vol. 7, no. 3, pp. 289–294, 1999.

[25] J. Schroeder, "Signal processing via Fourier-Bessel series expansion," *Digital Signal Processing*, vol. 3, no. 2, pp. 112–124, 1993.

[26] R. B. Pachori and P. Sircar, "EEG signal analysis using FB expansion and second-order linear TVAR process," *Signal Processing*, vol. 88, no. 2, pp. 415–420, 2008.

[27] E. D. Pisano, S. Zong, B. M. Hemminger, M. DeLuca, R. E. Johnston, K. Muller, M. P. Braeuning, and S. M. Pizer, "Contrast limited adaptive histogram equalization image processing to improve the detection of simulated spiculations in dense mammograms," *Journal of Digital Imaging*, vol. 11, no. 4, p. 193, 1998.
[28] R. C. Gonzales and R. E. Woods, "Digital image processing," 2002.
[29] X. Wu, D. Wang, J. Kurths, and H. Kan, "A novel lossless color image encryption scheme using 2D DWT and 6D hyperchaotic system," *Information Sciences*, vol. 349, pp. 137–153, 2016.
[30] K. He, X. Zhang, S. Ren, and J. Sun, "Deep residual learning for image recognition," in *Proceedings of the IEEE Conference on Computer Vision and Pattern Recognition*, 2016, pp. 770–778.
[31] J. Zhang, Y. Xie, Y. Li, C. Shen, and Y. Xia, "Covid-19 screening on chest X-ray images using deep learning based anomaly detection," *arXiv preprint arXiv:2003.12338*, 2020.
[32] E. E.-D. Hemdan, M. A. Shouman, and M. E. Karar, "Covidx-net: A framework of deep learning classifiers to diagnose covid-19 in X-ray images," *arXiv preprint arXiv:2003.11055*, 2020.
[33] T. Fawcett, "An introduction to ROC analysis," *Pattern Recognition Letters*, vol. 27, no. 8, pp. 861–874, 2006.
[34] C. K. Loo and M. Rao, "Accurate and reliable diagnosis and classification using probabilistic ensemble simplified fuzzy artmap," *IEEE Transactions on Knowledge and Data Engineering*, vol. 17, no. 11, pp. 1589–1593, 2005.